Applied Surface Science 343 (2015) 1–10

Contents lists available at ScienceDirect

Applied Surface Science

journal homepage: www.elsevier.com/locate/apsusc

Synthesis of magnetic graphene oxide–TiO_2 and their antibacterial properties under solar irradiation

Ying-Na Chang[a], Xiao-Ming Ou[b], Guang-Ming Zeng[a], Ji-Lai Gong[a,*], Can-Hui Deng[a], Yan Jiang[a], Jie Liang[a], Gang-Qiang Yuan[a], Hong-Yu Liu[a], Xun He[a]

[a] College of Environmental Science and Engineering, Key Laboratory of Environmental Biology and Pollution Control, Ministry of Education, Hunan University, Changsha 410082, PR China
[b] China National Engineering Research Center for Agrochemicals, Hunan Research Institute of Chemical Industry, Changsha 410014, PR China

ARTICLE INFO

Article history:
Received 3 January 2015
Received in revised form 12 March 2015
Accepted 14 March 2015
Available online 23 March 2015

Keywords:
Titanium dioxide
Graphene oxide
Antibacterial activity
Magnetic
Inorganic ions

ABSTRACT

Titanium dioxide (TiO_2) has been intensively researched and increasingly used as antibacterial agent, but it suffers from separation inconvenience. Its effective removal from water after reaction while maintaining its high antibacterial activity becomes necessary. In this work, it was the first time the magnetic graphene oxide–TiO_2 (MGO–TiO_2) composites were prepared through a simple synthesis method. The results indicated that MGO–TiO_2 exhibited a good antibacterial activity against *Escherichia coli*. MGO–TiO_2 was found to almost completely inactivate the *E. coli* within 30 min under solar irradiation. The effect of inorganic ions present in *E. coli* suspension was also evaluated. Compared with other ions, HCO_3^- and HPO_4^{2-} had a greater influence on the antibacterial property.

1. Introduction

The growing concerns about drinking water safety have put more stresses on the removal of pathogenic microorganisms [1]. Conventional disinfection methods such as chlorination and ozonation, are essential steps in centralized water-treatment. Despite their effectiveness in disinfection, these powerful oxidants may react with natural organic matter to form potentially mutagenic and carcinogenic disinfection by-products (DBPs) [2].

Photocatalytic inactivation is considered as a promising alternative for the removal of pathogens from water, as it can be potentially used without generating harmful by-products under solar irradiation. Titanium dioxide (TiO_2) is regarded as a suitable material because of its high catalytic activity, excellent chemical and thermal stability, low toxicity and cost [3,4]. Upon excitation by light, the photon energy generates electron–hole pairs on the TiO_2 surface, then the electrons and holes will react with oxygen and water molecules to form hydroxyl radicals (•OH), which are strong oxidants for disinfection of bacteria [5]. However, there are still many drawbacks. Firstly, a large bandgap (3.2 eV) of anatase TiO_2 restricts its use only to the narrow light-response range of ultraviolet (only 3–5% of total sunlight) [3]. Secondly, the low electron transfer rate and high electron recombination rate significantly limit the photo oxidation rate. Moreover, separation and reuse of the nano-TiO_2 pose another obstacle to practical application in drinking water [6].

Graphene oxide (GO) is chemically oxidized graphene, which attracts tremendous research interests due to its outstanding properties, including thermal and chemical stability, high mechanical strength, large specific surface area, good electron conductivity and water solubility [1]. The GO can effectively reduce the electron–hole recombination rate [3]. It has been reported that GO has excellent antibacterial performance, because GO generates reactive oxygen species and leads to DNA fragmentation [7].

In addition, a well-defined hybridized composites consisting of GO and TiO_2 was reported as an antimicrobial agent [1]. So far, all these studies on the antimicrobial properties of GO–TiO_2 were conducted in pure water under controlled laboratory conditions. Such studies ignored the interference of other substances in natural waters of nanometer materials. Therefore, more complex environments need to be investigated to determine the real effect of GO–TiO_2 on the bacteria.

With the rapid development of nanotechnology and increasing usage of nanoparticles, a new crisis has emerged (i.e. nanotoxicology). Chen et al. [8] observed that TiO_2 nanoparticles could induce DNA double strand breaks in bone narrow cells. Therefore, it is essential to remove the nanoparticles from aqueous solution, and

* Corresponding author. Tel.: +86 731 88822829; fax: +86 731 88822829.
E-mail address: jilaigong@gmail.com (J.-L. Gong).

http://dx.doi.org/10.1016/j.apsusc.2015.03.082
0169-4332/

a good choice to introduce magnetic nanoparticle into the nanometer antibacterial material.

The magnetic nanoparticles not only have the characteristics of nano-materials, but also have another important property- magnetism [9]. Iron-based magnetic nanoparticles have been used for an increasing number of environmental application [10]. It is worth mentioning that magnetic iron oxide nanoparticles also have the ability of bacterial inactivation. Auffan et al. [10] reported antimicrobial properties of Fe_3O_4 and γ-Fe_2O_3 nanoparticles toward the Gram-negative bacterium *Escherichia coli* and proved the release of Fe^{2+} from Fe_3O_4 and γ-Fe_2O_3 nanoparticles causing cytotoxicity. In our previous work, iron oxide loaded graphene nano-composites were prepared and its inactivation performance and mechanism of *E. coli* were reported [11].

This work reported a series of antibacterial nano-materials using a simple preparation method, by introducing TiO_2 and iron oxide magnetic (M) nanoparticles into GO nanosheets. Magnetic graphene oxide–TiO_2 (MGO–TiO_2) nanomaterials possessed the antimicrobial properties of three materials including TiO_2, GO and magnetic nanoparticles and the separation convenience of magnetic nanoparticles. *E. coli* were used to evaluate the bactericidal property of the nano-composite under solar irradiation, because *E. coli* was often used for microbial indicators of drinking water monitoring. The optimal TiO_2 content in antibacterial nanomaterials was investigated. The nano-composites proposed in this work conquered the drawbacks of TiO_2, integrated the advantages of each respective component and possessed more superior merits over previous TiO_2-based antibacterial agent, including: (1) suppressing recombination of photo-generated electron–hole pairs through an effective charge transfer route from TiO_2 to GO, (2) providing additional antibacterial property with GO and iron oxide magnetic nanoparticles, and (3) easy separation from water owing to magnetic nanoparticles.

To our knowledge, no reports were found to synthesize multifunctional MGO–TiO_2 nanocomposites and used it for water disinfection under solar irradiation. In addition, the interferences from some common anions (i.e. HCO_3^-, Cl^-, SO_4^{2-}, NO_3^- and HPO_4^{2-}) and cations (i.e. K^+ and Na^+) in natural water were also investigated.

2. Experimental

2.1. Materials

Graphite powders were purchased from Jim-Shan-Ting New Chemical Factory (Shanghai, China). TiO_2 nanoparticles were used from Shanghai Aladdin Reagent Company (Shanghai, China). Sodium nitrate ($NaNO_3$), sulfuric acid (H_2SO_4, 98%), potassium permanganate ($KMnO_4$), hydrogen peroxide (H_2O_2, 30%), ferrous ammonium sulfate [$NH_4Fe(SO_4)_2{\cdot}12H_2O$], ammonium ferric sulfate [$(NH_4)_2SO_4{\cdot}FeSO_4{\cdot}6H2O$], ammonia solution ($NH_3$, 25%) methanol ($CH_3OH$, 99.9%) and absolute ethanol (CH_3CH_2OH) were obtained from Sinopharm Chemical Reagent Company (Shanghai, China). Sodium hydrogen phosphate (Na_2HPO_4), sodium bicarbonate ($NaHCO_3$), sodium sulfate (Na_2SO_4), sodium chloride (NaCl), potassium sulfate (K_2SO_4) and potassium bicarbonate ($KHCO_3$) were supplied by Sinopharm Chemical Reagent Company (Beijing, China). All chemicals were analytical grade.

2.2. Preparation of GO

GO was prepared according to the Hummers' method [12–14]. Graphite powders (1 g) and $NaNO_3$ (0.5 g) were added to concentrated H_2SO_4 (23 mL) in a 1 L conical flask. Under ice bath condition, $KMnO_4$ (3 g) was added slowly with stirring, and the temperature of the mixture was kept at below 10 °C. Once the mixture was homogeneous, it was transferred to an oil bath maintained at 35 °C and stirred for 30 min. Then the dispersion was diluted with 46 mL of warm ultrapure water (about 30 °C) to form a brownish mixture, and the mixture was stirred for 30 min as the temperature was increased to 98 °C, with subsequent addition of warm ultrapure water (140 mL), followed by slow addition of H_2O_2 (2.5 mL). The color of the suspension changed from brown to yellow. The suspension was filtered through a 0.1 μm filter membrane, and washed with ultrapure water and absolute ethanol sequentially until the pH of the supernatant was 7. The GO samples were recovered finally and then dried in a vacuum desiccator.

2.3. Preparation of MGO

GO (1.0 g) described above was dispersed in ultrapure water (100 mL) using ultrasonic treatment for 30 min to obtain GO suspension. Under N_2 atmosphere, $(NH_4)_2SO_4{\cdot}FeSO_4{\cdot}6H_2O$ (5.8 g) and $NH_4Fe(SO_4)_2{\cdot}12H_2O$ (10.7 g) were added to ultrapure water (100 mL) (molar ratio of 1.5:1 for Fe^{3+} and Fe^{2+}). Then mixed iron solution was quickly added with ammonia (10 mL), with subsequent addition of GO suspension with stirring in the water bath pot at 85 °C for 45 min. Finally, the product was separated using the magnet and washed with ultrapure water and absolute ethanol until the pH was 7. The resulting MGO was dried in a vacuum oven at 60 °C for 12 h.

2.4. Preparation of MGO–TiO_2

Firstly, various concentrations of TiO_2 dispersion were prepared by adding different amount of TiO_2 power (0.5, 1.0, and 1.5 g) in 100 mL ultrapure water and shaked for 30 min by ultra-sonication. The synthesis process of MGO–TiO_2 was similar to that of MGO, except that TiO_2 dispersion and iron salts were simultaneously added in the GO solution during the preparation of MGO–TiO_2. According to the different amounts of TiO_2, the final drying products were marked as MGO–TiO_2-1, MGO–TiO_2-2 and MGO–TiO_2-3, respectively.

2.5. Characterization

Field emission scanning election microscopy (FESEM) images were obtained using a JSM-6700FLV microscope. Transmission electron microscopy (TEM) was performed using a JEM-3010. Energy dispersive X-ray (EDS) measurement was conducted using the EDAX system attached to the same field emission scanning electron microscopy (JSM-6700FLV). The structure phases of the synthesized antibacterial materials were analyzed by X-ray diffraction (XRD) (D/max 2550 X-ray diffractometer, Rigaku, Japan). The analysis of elements and function groups on the surface of MGO–TiO_2-2 was determined using X-ray photoelectron spectroscopy (XPS, Thermo Scientific Escalab 250Xi) with a Mg Kα X-ray source (1254 eV of photons). The absorbance of the nanomaterials solutions during the tests was analyzed in a UV–Vis spectrophotometer (Shimadzu UV-2550). Lake shore 7410 vibrating sample magnetometer (VSM) was employed to record the magnetization curve.

2.6. Bacterial strain and growth culture media

The bacteria strain *E. coli* ATCC 25922 was purchased from the China Center for Type Culture Collection (Beijing, China). Before the experiment, all glasswares and solutions used in the experiments were autoclaved at 121 °C for 15 min.

The bacterial strain was grown in Luria-Bertani (LB) medium (yeast extract 5 g, tryptone 10 g and NaCl 5 g in 1 L of deionized

water at PH of 7.0) at 37 °C for 24 h. *E. coli* cells were then collected by centrifugation followed by multiple washing cycles. After decanting the supernatant, the bacteria cells were re-suspended in sterile water to achieve the desired initial concentrations. The *E. coli* stock solution of approximately 1×10^5–1×10^6 colony forming units per mL (cfu/mL) was then prepared for the anti-bacterial study.

2.7. Antibacterial activity tests

The following three kinds of tests were performed to evaluate the antimicrobial properties. The first experiment was to explore the antimicrobial properties of different materials. The suspension (50 mL) containing 0.01 g samples (i.e. solar only (no catalysts), TiO_2, MGO, MGO–TiO_2-1, MGO–TiO_2-2 and MGO–TiO_2-3, MGO–TiO_2-2 in the dark) and *E. coli* (1×10^5–1×10^6 cfu/mL) was stirred for 90 min. The second experiment was to further find out the most effective concentration of the most optimal antibacterial material described in the first experiment. Six different concentrations (from 100 to 200 mg/L) of this antibacterial material were studied after 30 min reaction. Finally, the interferences from major inorganic species in natural water (i.e. HPO_4^{2-}, HCO_3^-, NO_3^-, SO_4^{2-}, Cl^-, K^+, Na^+) on the antibacterial property of this material were elucidated by introducing appropriate amounts of Na_2HPO_4, $NaHCO_3$, $NaNO_3$, Na_2SO_4, NaCl, K_2SO_4 and $KHCO_3$ into the suspension. The concentrations of these ions were 0.2, 0.4, 0.6, 0.8 and 1.0 mM, respectively.

All the above experiments were carried out under a solar simulator irradiation (Xenon arc lamp, Newport Oriel, 100 mW/cm^2). Nanoparticle suspensions were freshly prepared in ultrapure water and were both sonicated for 30–35 min to ensure good dispersion before each experiment. In the process of sampling, 100 μL of each bacterial suspension was taken out. Samples were serially diluted in sterile water and plated. Every sample was diluted at 1/10 relationship up to appropriate dilutions and consequently plated on Eosin-methylene blue agar. Inoculated samples were incubated at 37 °C for 24 h before counting. Eosin-methylene blue agar is a selective media, specific for the detection of coliforms. The experiment was carried out in the environment, in order to prevent other bacterial in environment interference results at last count, eosin-methylene blue agar was used as a way to suppress growth of other organisms.

The detection limit for this method of quantification is 10 cfu/mL. The following equations were used to represent antibacterial activity:

$$\text{Antibacterial rate} = \left(\frac{N_t}{N_0}\right) \times 100\% \quad (1)$$

where N_0 and N_t and are the viable cells count before and after irradiation, respectively.

3. Results and discussion

3.1. Characterization of as-prepared photocatalysts

The surface morphology of samples was presented by SEM and TEM. Fig. 1 showed SEM images of TiO_2, GO, MGO and MGO–TiO_2-2. TiO_2 image indicated that TiO_2 was nearly spherical particles. GO clearly showed the typical wrinkle characterization. Spherical and stick magnetic particles covered on the surface of GO. The MGO–TiO_2-2 image indicated that the GO surface was clearly decorated with particles.

To further investigate the nanoparticles more clearly, TEM was used to characterize the morphologies of TiO_2, GO, MGO and MGO–TiO_2-2 (Fig. 2). Sheets with wrinkled surfaces were clearly visible in GO, MGO and MGO–TiO_2-2 composites. The size distribution of TiO_2, MGO and MGO–TiO_2-2 nanoparticles was shown in Fig. 3, the size distribution of three particles including TiO_2, MGO and MGO–TiO_2-2 were nearly 44.87, 12.09 and 13.69 nm, respectively. This can be explained that pure TiO_2 particles were easily aggregated. When TiO_2 particles were supported on GO surface, the rippled and resemble crumpled silk veil waves of GO were appropriate for immobilizing TiO_2 nanoparticles, thus reducing TiO_2 agglomeration [15].

EDS spectra showed that the elements of carbon, oxygen and iron were obtained in MGO nano-composite (see Fig. 4a), and both TiO_2 and iron oxide particles were successfully coated on GO surface (see Fig. 4b–d). Table 1 listed element contents of MGO, MGO–TiO_2-1, MGO–TiO_2-2 and MGO–TiO_2-3. Results showed that Ti contents (wt%) of MGO–TiO_2-1, MGO–TiO_2-2 and MGO–TiO_2-3

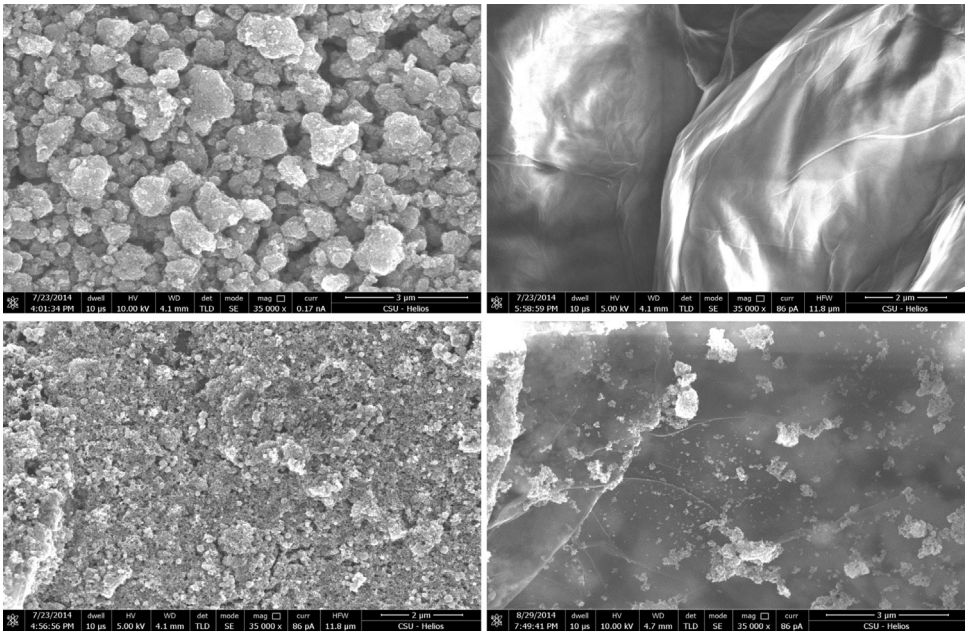

Fig. 1. SEM images of nanoparticles. Top left TiO_2, top right GO, bottom left MGO, bottom right MGO–TiO_2-2.

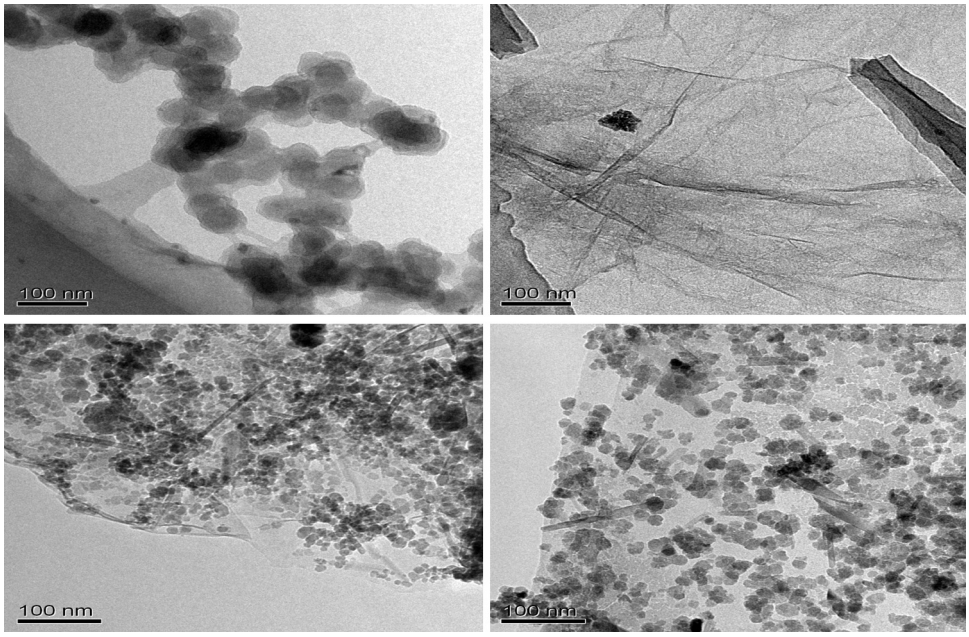

Fig. 2. TEM images of nanoparticles. Top left TiO_2, top right GO, bottom left MGO, bottom right MGO–TiO_2-2.

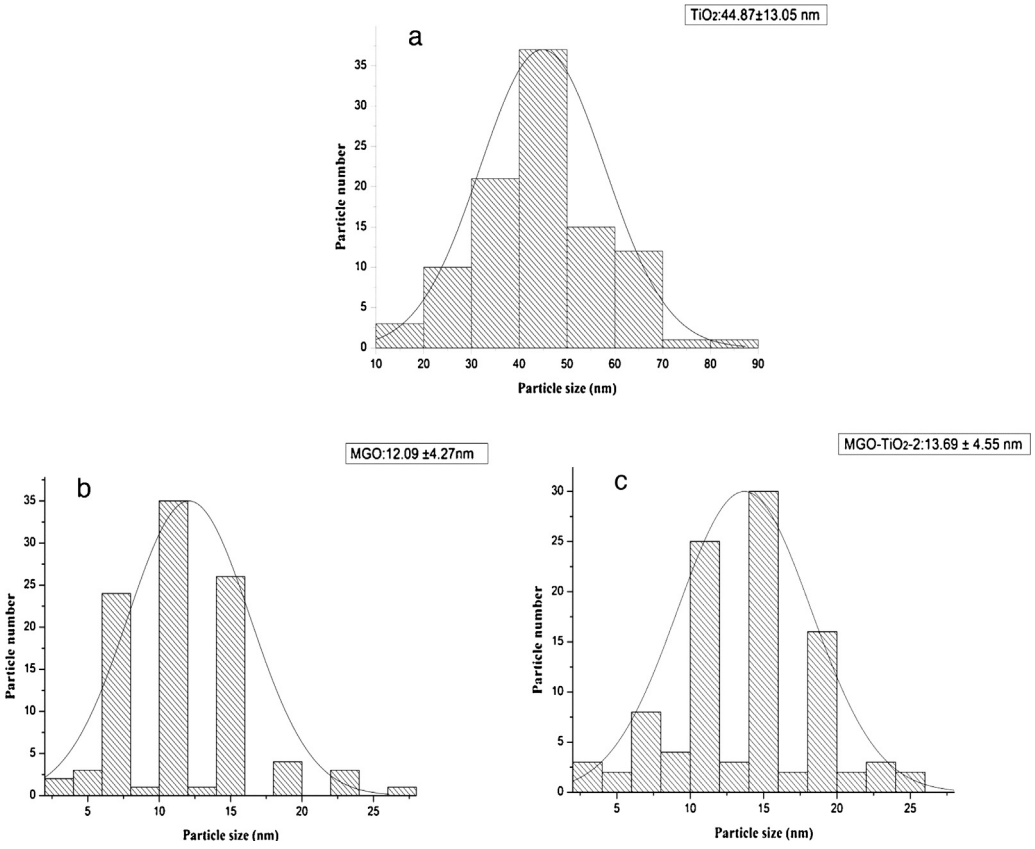

Fig. 3. Size distribution histograms. (a) TiO_2, (b) MGO and (c) MGO–TiO_2-2.

were 4.79%, 6.02% and 8.21%, respectively. Besides, it was observed that the amount of TiO_2 and magnetic nanoparticles varied with various kinds of MGO–TiO_2 nano-composite.

The X-ray diffraction (XRD) patterns of GO, TiO_2, MGO and MGO–TiO_2-2 were displayed in Fig. S1. In the XRD patterns (Fig. S1a) of GO nanosheet, the diffraction peak located at 9.98°, corresponding to the typical diffraction peak of GO nanosheets. Certain peaks observed in the TiO_2 diffraction pattern (Fig. S1b) were related to the anatase phase at 25.3°, 36.9°, 48.0°, 54.2°, 54.6°, 62.3° and 70.0° [11,16]. The peaks (Fig. S1c) at 2θ values of 24.3°, 33.0°, 35.6°, 40.2°, 49.9°, 62.1° and 64° were assigned to maghemite or magnetite, and the peaks at 2θ = 18.4°, 30.1°, 43.6°, 53.9° and 62.5° were attributed to hematite [17]. It was noted that the characteristic peak of GO at 2θ = 9.98° was obviously reduced in the XRD

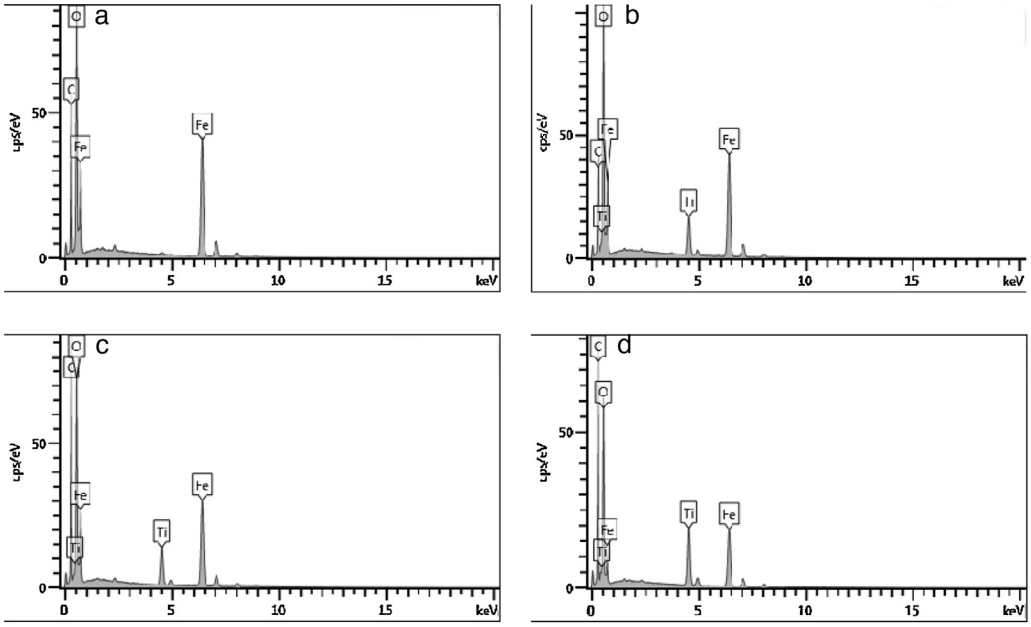

Fig. 4. EDS spectra of nano-composites. (a) MGO, (b) MGO–TiO_2-1, (c) MGO–TiO_2-2 and (d) MGO–TiO_2-3.

Table 1
Elemental compositions of MGO–TiO_2-1, MGO–TiO_2-2 and MGO–TiO_2-3.

Element	MGO (wt%)	MGO–TiO_2-1 (wt%)	MGO–TiO_2-2 (wt%)	MGO–TiO_2-3 (wt%)
C	34.06	39.96	24.18	40.92
O	29.84	30.65	34.48	32.58
Fe	36.10	24.60	35.33	18.29
Ti	0.00	4.79	6.02	8.21
Totals	100	100	100	100

patterns of MGO, which could be caused by the reasons as follows: The weak peaks of carbon in MGO and MGO–TiO_2-2 (Fig. S1d) resulted from the aggregation reduction of graphene sheets, the increase of monolayer graphene in the presence of magnetite and the strong peaks of the M nanoparticles overwhelming the weak carbon peaks. The results in our work were consistent with the previous studies [11].

Fig. S2a shows the XPS analysis in MGO–TiO_2-2 nanomaterial. For MGO–TiO_2-2, the C 1s XPS spectrum can be devolved into two peaks at 284.5 and 287 eV, corresponding to the non-oxygenated carbon (sp2 hybridized C—C bonds), the epoxyl and alkoxyl carbon (C═O bonds) in the graphene oxide structure, respectively [15]. In O 1s spectra of GO (shown in Fig. S2c), the main peaks at 530.1 and 532.5 eV were assigned C—O bonds and Ti—O on the GO surface [18]. The binding energies of Fe2p3/2 and Fe 2p1/2 were 711.2 and 725.7 eV (Fig. S2d), respectively. The peaks of Fe 2p appeared in MGO–TiO_2-2 nanomaterial further illustrating iron oxide nanoparticles were successfully coated on GO nanosheet. The satellite peak of Fe 2p3/2 for MGO–TiO_2-2 located at 719.5 eV, which was consistent with the previous report [17]. From the XPS curves of Ti 2p region (shown in Fig. S2e), two peaks were detected and centered at 459.5 and 465.3 eV, corresponding to Ti 2p3/2 and Ti 2p1/2 of the Ti^{4+} chemical state in TiO_2 lattice, respectively [15].

The UV–Vis spectroscopy can be used to determine the change in the absorption of the TiO_2 and its compounds. The absorbance spectra of the TiO_2, MGO–TiO_2-1, MGO–TiO_2-2 and MGO–TiO_2-3 were depicted in Fig. S3. It was obvious that the composite samples (i.e. MGO–TiO_2-1, MGO–TiO_2-2 and MGO–TiO_2-3) showed red-shifts of absorption edges compared to pure TiO_2. This result indicated that the composite samples could utilize visible light for photocatalytic antibacterial application.

The magnetic properties of the four types nanoparticles (i.e. MGO, MGO–TiO_2-1, MGO–TiO_2-2 and MGO–TiO_2-3) were measured by VSM analysis at room temperature. The measured magnetization curves were depicted in Fig. 5a. The results showed that the saturation magnetization values of MGO, MGO–TiO_2-1, MGO–TiO_2-2 and MGO–TiO_2-3 nanoparticles were 30.03, 32.56, 33.85 and 28.68 emu/g, respectively. It was reported that saturation magnetization of 16.30 emu/g was sufficient for magnetic separation [14,19].

As demonstrated in Fig. 5b, after dispersing magnetic nanoparticles in aqueous solution, the black particles were rapidly attracted toward a magnet within few seconds, indicating that all of them could be separated from aqueous solution by a magnet.

3.2. The antimicrobial properties of different materials

The photo-catalytic inactivation of *E. coli* by different materials under solar simulator irradiation was presented in Fig. 6. In the first 10 min, MGO was the best antimicrobial properties, which inactivated rate was 48.23% of the *E. coli*. However, from the time 10 min and 20 min, the *E. coli* survival rates decreased sharply for MGO–TiO_2-1 (from 82.18% to 4.3%) and MGO–TiO_2-2 (from 90% to 2.83%). After 20 min, the bacteria survival rate was in the order: MGO–TiO_2-2 > MGO–TiO_2-1 > MGO > MGO–TiO_2-3 > TiO_2 > dark > light. At 30 min, the antibacterial rates were 24.61% (dark), 24.22% (light) 39.27% (TiO_2), 66.09% (MGO–TiO_2-3), 73.82% (MGO), 98.85% (MGO–TiO_2-1) and 99.60% (MGO–TiO_2-2). Our previous results showed that antimicrobial properties of MGO–TiO_2 in the dark were related to toxicity of Fe^{2+} [11]. After 90 min solar irradiation, there were 99.67%, 99.99% and 99.99% inhibition of *E. coli* in the presence of MGO, MGO–TiO_2-1 and MGO–TiO_2-2, respectively. Antimicrobial properties of MGO, on one hand, was partly from Fe_3O_4 and graphene oxide [11,20], on the other hand, was partly from the simulated solar light. While the light, dark, TiO_2 and MGO–TiO_2-3 bacterial inactivation rates were only 59.04%, 64.53%, 76.23% and 94.21%, respectively. On the one hand, the excellent antibacterial activity of MGO–TiO_2-1 and MGO–TiO_2-2 nano-composites could be attributed to the efficient separation of

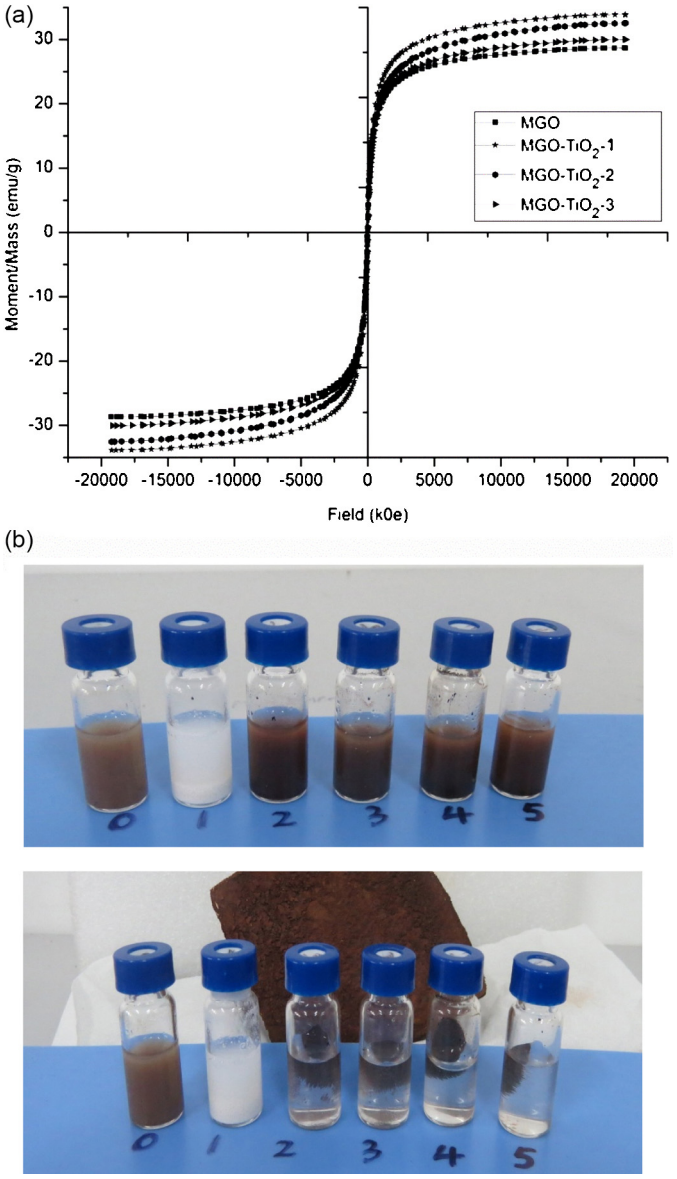

Fig. 5. (a) VSM measurements for magnetic nanoparticles, (b) the magnetic separation of magnetic nanoparticles by magnet (i.e. 0: GO, 1: TiO_2 2: MGO, 3: MGO–TiO_2-1, 4: MGO–TiO_2-2 and 5: MGO–TiO_2-3).

photo-generated electron–hole pairs, since GO could be used as an electron acceptor and transporter [21], suggesting that more •OH involved in the antibacterial activity. On the other hand, the MGO and TiO_2 had a synergism of inhibiting *E. coli*.

The inactivation model fitting tool (Eq. 2) was used for analyzing antimicrobial properties of different materials. The inactivation rate constants obtained from fitting the kinetics data with the model are shown in Table 2

$$N_t = N_0 \times e^{(-kt)} \quad (2)$$

where k is the rate constant (min^{-1}) and N_0 and N_t are the viable cells count at time zero and t.

The inactivation rate was found to increase with the TiO_2 content on MGO. For the MGO, MGO–TiO_2-1 and MGO–TiO_2-2, the rate constants were 0.059, 0.073 and 0.098 min^{-1}, respectively. The inactivation rate constant for MGO–TiO_2-2 (0.098 min^{-1}) showed a 5.5-fold increase from the TiO_2 (0.015 min^{-1}). Also shown in Table 2 is the time required for each nanomaterial to achieve 4 log

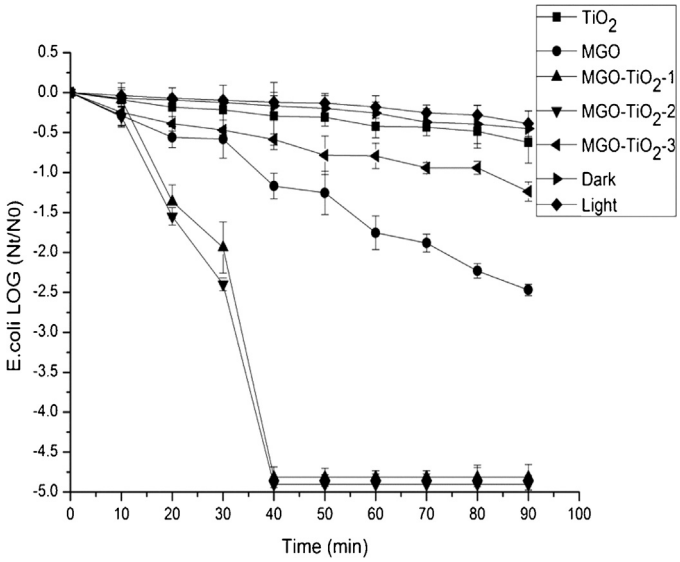

Fig. 6. Photo-catalytic antimicrobial properties of *E. coli* on different materials under solar simulator irradiation. Light: solar only (no catalysts), dark: MGO–TiO_2-2 in the dark (material concentration: 200 mg/L; initial bacteria concentration: 10^5–10^6 cfu/mL; solar intensity: 100 mw/cm^2).

Table 2
The inactivation rate constants for different materials.

Material	Rate constant (min^{-1})	R^2	Time required to achieve 4 log removal (min)
Dark	0.011	0.97	363.64
Light	0.008	0.95	500.00
TiO_2	0.015	0.98	266.67
MGO	0.059	0.99	67.80
MGO–TiO_2-1	0.073	0.80	54.79
MGO–TiO_2-2	0.098	0.95	40.82
MGO–TiO_2-3	0.035	0.97	114.29

removal of *E. coli*. MGO–TiO_2-2 antimicrobial property is the best, 4 log removal of *E. coli* could be obtained in 41 min.

It was illustrated that the antibacterial activities of MGO, MGO–TiO_2-1 and MGO–TiO_2-2 nano-composites were related to TiO_2 content in the nano-composites. The bacterial inactivation rates increased with increasing TiO_2 content in the nano-composites. The reason was that more amount of TiO_2 generated more •OH.

Noticeably, the MGO–TiO_2-2 showed the highest photo-catalytic antibacterial activity. A further increase of TiO_2 nanoparticles had no favorable effect on the antimicrobial activity of the nano-composites. This result can be explained as follows: a large number of TiO_2 existed in the GO, the GO might be covered by TiO_2 nanoparticles, which could lead to a shield of the active sites of GO during the antibacterial process [22]. Thus, the samples of MGO–TiO_2-3 had a lower activity than MGO–TiO_2-1 and MGO–TiO_2-2.

The potential mechanism for the enhanced *E. coli* antibacterial rate of MGO–TiO_2-2 was due to the higher •OH production rate. To test this mechanism, methanol was used as •OH scavengers [23,24]. Experiment was performed using MGO–TiO_2-2 with different methanol concentrations. Fig. 7 pointed out that the bacterial survival rates increased with the increase of the methanol concentration. The bacterial survival rates at 30 min were 0.01%, 15.58%, 16.48%, 19.75% and 24.26% when the methanol concentrations were 0, 30, 100, 200 and 400 mM, respectively. This could be explained that much more methanol would remove more •OH, and cause the increased bacterial survival rates. The data suggested that •OH

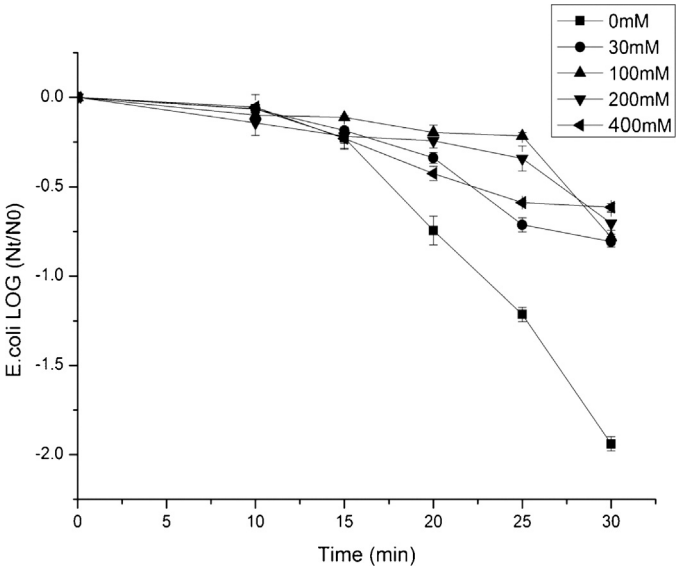

Fig. 7. The antimicrobial properties in the presence of methanol (MGO–TiO_2-2 concentration: 200 mg/L; initial bacteria concentration: 10^5–10^6 cfu/mL; solar intensity: 100 mw/cm^2).

played an important role in *E. coli* inactivation. This agreed with the conclusions by other reports [23,24].

3.3. The most effective concentration of MGO–TiO_2-2

Fig. 8 showed the effects of MGO–TiO_2-2 concentration on photo-killing of *E. coli* under sunlight after 30 min exposure time. When the concentration of MGO–TiO_2-2 was between 100 and 200 mg/L, the bacterial survival rate decreased with the increasing MGO–TiO_2-2 concentration. At 30 min, the bacterial survival rates were 33.06%, 25.14%, 7.5%, 6.09%, 1% and 1.15% when the MGO–TiO_2-2 concentrations were 100, 120, 140, 160, 180 and 200 mg/L, respectively. This result could be attributed to that the more MGO–TiO_2-2 produced more •OH. But when the concentration was above 180 mg/L, the bacteria survival rate no longer changed. The increase of material concentration did not enhance the antibacterial rate, which may be derived from two possible reasons. Firstly, the higher the concentration of MGO–TiO_2-2, material more easily agglomerated leading to the contact of nanomaterials and bacteria reduced [25,26]. To test this mechanism, the particle size of materials in the water was analyzed by using a Zetasizer (Meter 3.0). Mean hydrodynamic diameters of all photocatalyst suspensions in sterile water are presented in Fig. 9. The results found that no matter before or after the reaction, the particle size of 180 mg/L was significantly lower than the other concentrations. Secondly, available oxygen was probably consumed at the beginning of experiment due to rapid photo-catalytic reaction and was insufficient to support further photo-catalytic reaction [25]. Dissolved oxygen meter (Oxi3210) was used to measure the concentration of dissolved oxygen in solution. The results are shown in Fig. 10. Compared with other concentration, when the concentration of MGO–TiO_2-2 is 200 mg/L, the dissolved

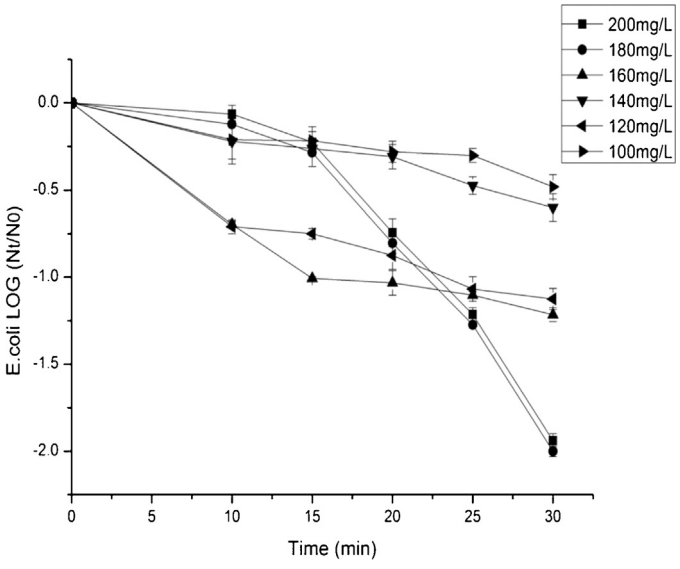

Fig. 8. Effects of MGO–TiO_2-2 concentration on photo-killing of *E. coli* under sunlight after 30 min exposure time (initial bacteria concentration: 10^5–10^6 cfu/mL; solar intensity: 100 mw/cm^2).

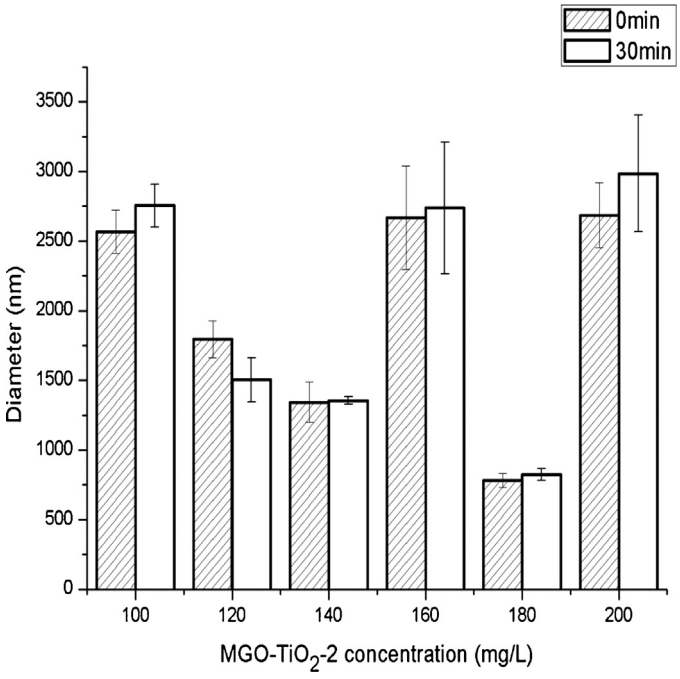

Fig. 9. Dispersed particle diameters of MGO–TiO_2-2 nanoparticles in different concentrations (0 min: the initial particle size of MGO–TiO_2-2, 30 min: the particle size of MGO–TiO_2-2 after 30 min).

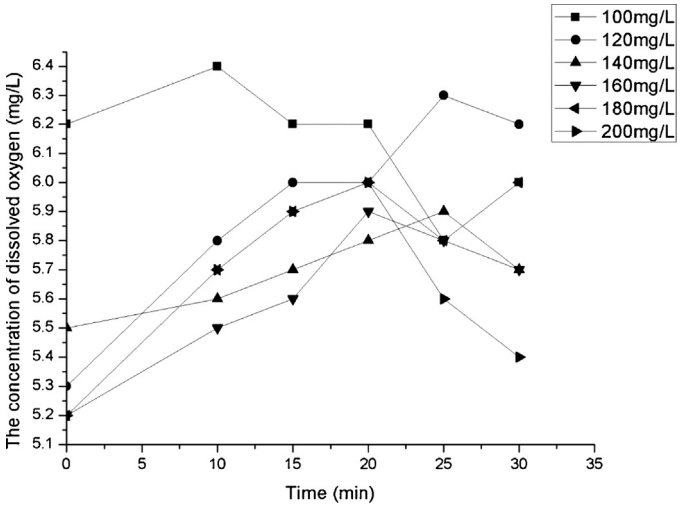

Fig. 10. The dissolved oxygen contents of MGO–TiO_2-2 nanoparticles in different concentrations.

oxygen concentration decreased sharply after 20 min. Therefore, the hypothesis is consistent with the experimental results. As a result, the most effective concentration of MGO–TiO_2-2 was 180 mg/L.

3.4. The influence of inorganic ions on E. coli survival

Fig. 11 indicated that *E. coli* inactivation in the presence of different anions with different concentrations.

All the inorganic anions had influences on the antibacterial activity of MGO–TiO_2-2. However, effects of different anions were different at the same concentration. Effects of the same anions in different concentrations were also different. The experimental results were shown in Table 3a. The bacterial survival rates in the presence of HPO_4^{2-}, SO_4^{2-}, Cl^-, HCO_3^-, NO_3^-, K^+ and Na^+ with different concentrations were presented in Figs. S1–S7. Results showed that, HCO_3^- and HPO_4^{2-} decreased the inactivation rates in a larger extent than Cl^-, SO_4^{2-} and NO_3^-.

For HCO_3^-, this phenomenon can be explained by following reasons: HCO_3^- captured the h^+ produced by TiO_2 (Eq. R1). Furthermore, HCO_3^- reacted with the •OH (Eq. R2) and produced the less reactive anion radical $CO_3^{\bullet-}$. In addition, HCO_3^- could absorb a part of light, which limited the light penetration into the bacterial suspension [27]

$$HCO_3^- + h^+ \rightarrow HCO_3^{\bullet-} \quad (R1)$$

$$^{\bullet}OH + HCO_3^- \rightarrow CO_3^{\bullet-} + H_2O \quad (R2)$$

HPO_4^{2-} produced the largest negative effect on the nanocomposite disinfection of all the studied anions. The greater the concentration of HPO_4^{2-}, the greater the survival rate of bacteria. Rincon [27] thought that once the HPO_4^{2-} entered the water, HPO_4^{2-} rapid adhered to the surface of TiO_2. Thus, the inactivated catalyst could not produce •OH to attack bacteria. Moreover, HPO_4^{2-} also absorbed exciting light.

Compared with other ions, Cl^- had a minimum effect of antibacterial property. This phenomenon could be explained that although Cl^- scavenged the •OH (Eq. R3) and blocked the photoactive sites of the MGO–TiO_2-2 surface, thus reducing the MGO–TiO_2-2 antibacterial property [2]. However, Kang et al. pointed that bacteria metabolic process could produce chloride radicals ($Cl^{\bullet}$), Cl^- could react with $Cl^{\bullet}$ and rapidly equilibrated with dichloride radical anion ($Cl^{\bullet-}$) (Eq. R4), the $Cl^{\bullet-}$ also was a disinfectant, therefore, accelerating the deactivation rate [27–29]

$$^{\bullet}OH + Cl^- \rightarrow Cl^{\bullet} + OH^- \quad (R3)$$

$$Cl^{\bullet} + Cl^- \rightarrow Cl^{\bullet-} \quad (R4)$$

Alrousan et al. showed that SO_4^{2-} and NO_3^- anions would stick to the surface on TiO_2 via physical forces as Van der Waals force and hydrogen bond. Therefore, the addition of SO_4^{2-} and NO_3^- led to the inhibition of *E. coli* inactivation [27,30]. In addition, it can be seen from Fig. 12 that SO_4^{2-} had a greater effects on antimicrobial properties of the material. The phenomenon indicated that SO_4^{2-} was more easily adsorbed on MGO–TiO_2-2 than NO_3^- [30].

Table 3b showed that, except HPO_4^{2-}, the concentration of other ions was unrelated to the inhibition. Furthermore, due to the high adsorption on TiO_2 surface and negatively charge of anions, they formed a negatively charged layer on the surface of catalyst, which repulsed bacteria, causing a decrease in the disinfection rate.

Fig. 12 displayed the inactivation rates when Na^+ and K^+ were in the *E. coli* suspension. Compared with $NaHCO_3$ and Na_2SO_4, regardless of the concentration of Na^+, effect of $NaHCO_3$ bacteria survival rates were always higher than Na_2SO_4. $KHCO_3$ and K_2SO_4 also showed the same result. $NaHCO_3$ and $KHCO_3$ made the

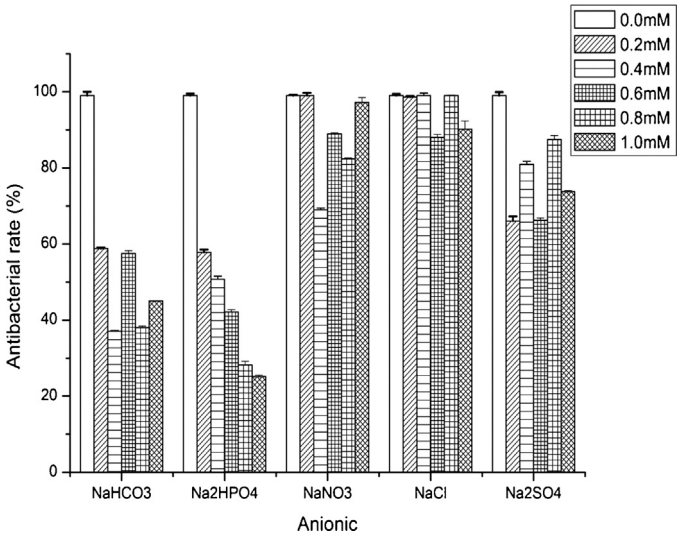

Fig. 11. *E. coli* antimicrobial properties in the presence of different anions with different concentrations (MGO–TiO_2-2 material concentration: 180 mg/L; initial bacteria concentration: 10^5–10^6 cfu/mL; solar intensity: 100 mw/cm^2; irradiation time: 30 min).

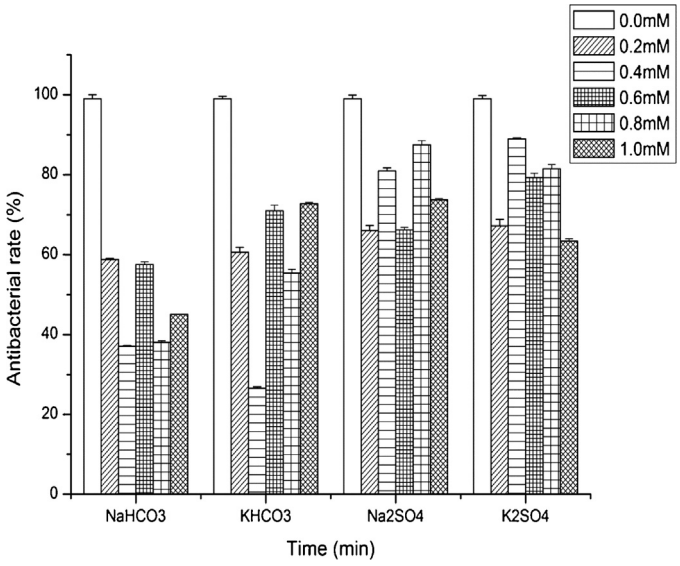

Fig. 12. *E. coli* antimicrobial properties in the presence of K^+ and Na^+ under different concentrations (MGO–TiO_2-2 material concentration: 180 mg/L; initial bacteria concentration: 10^5–10^6 cfu/mL; solar intensity: 100 mw/cm^2; irradiation time: 30 min).

Table 3a
Effects of different anions at the same concentrations.

Anion concentration (mM)	The interference order of MGO–TiO_2-2
0.2	$HPO_4^{2-} > HCO_3^- > SO_4^{2-} > Cl^- > NO_3^-$
0.4	$HCO_3^- > HPO_4^{2-} > NO_3^- > SO_4^{2-} > Cl^-$
0.6	$HPO_4^{2-} > HCO_3^- > SO_4^{2-} > Cl^- > NO_3^-$
0.8	$HPO_4^{2-} > HCO_3^- > NO_3^- > SO_4^{2-} > Cl^-$
1.0	$HPO_4^{2-} > HCO_3^- > SO_4^{2-} > Cl^- > NO_3^-$

Table 3b
Effects of same anions in different concentrations.

Anion type	The interference order of MGO–TiO_2-2
HCO_3^-	0.4 mM > 0.8 mM > 1.0 mM > 0.6 mM > 0.2 mM
Cl^-	0.6 mM > 1.0 mM > 0.2 mM > 0.4 mM > 0.8 mM
SO_4^{2-}	0.2 mM > 0.6 mM > 1.0 mM > 0.4 mM > 0.8 mM
NO_3^-	0.4 mM > 0.8 mM > 0.6 mM > 1.0 mM > 0.2 mM
HPO_4^{2-}	1.0 mM > 0.8 mM > 0.6 mM > 0.4 mM > 0.2 mM

bacterial disinfection rate decreased significantly mainly due to the presence of HCO_3^-. This was well agreement with experimental result obtained from Fig. 11, HCO_3^- on disinfection rate were much higher than SO_4^{2-}. In addition, the effects of K^+ and Na^+ on bacteria survival rates had no regular tendency at different concentrations. This indicated that, in the process of MGO–TiO_2-2 sterilization, K^+ and Na^+ also had effects on the *E. coli* disinfection rate. The effects were attributed to the changes of *E. coli* cell permeability and the leakage of ions inside the bacterial cell [27,31–33].

4. Conclusions

The antibacterial properties of magnetic graphene oxide–TiO_2 were investigated and the influence of inorganic ions under solar irradiation was discussed. The conclusions were showing as follows:

(1) A simple method of immobilizing TiO_2 and iron-based magnetic nanoparticles onto the surface of GO was presented in this work. Three kinds of composite materials (i.e. MGO–TiO_2-1, MGO–TiO_2-2 and MGO–TiO_2-3) were generated by adjusting the content of TiO_2. SEM and TEM images proved that TiO_2 and magnetic nanoparticles were uniformly grown on the GO sheets.
(2) MGO–TiO_2-2 achieved the most excellent antimicrobial property in comparison with other adopted photo-catalysts. After 30 min solar irradiation, the bacterial inactivation rate nearly achieved 100%. The most effective concentration was only 180 mg/L. The outstanding antibacterial performance of MGO–TiO_2-2 was attributed to the synergistic effect of MGO and TiO_2.
(3) The addition of inorganic ions reduced antibacterial properties of MGO–TiO_2-2. HCO_3^- and HPO_4^{2-} had a great influence on the antibacterial property compared with SO_4^{2-}, Cl^-, NO_3^-, K^+ and Na^+. The main reason was that HCO_3^- and HPO_4^{2-} could react with $^{\bullet}OH$.
(4) The saturation magnetization was 33.87 emu/g. It could rapidly be separated from aqueous solution when the magnetic field was applied.

The low cost of GO and TiO_2, the simplicity of MGO–TiO_2-2 manufacturing procedure, separation convenience and its effective antibacterial properties indicate that MGO–TiO_2-2 is a promising candidate in water disinfection treatment.

Acknowledgments

The authors are grateful for the financial supports from National Natural Science Foundation of China (51039001, 50978088, 50808070, 21275044, 51479072 and 51108166), China National Science and Technology Support Program (2011BAE06A01), the Interdisciplinary Research Funds for Hunan University and the Scientific Research Foundation for the Returned Overseas Chinese Scholars, State Education Ministry.

Appendix A. Supplementary data

Supplementary data associated with this article can be found, in the online version, at http://dx.doi.org/10.1016/j.apsusc.2015.03.082.

References

[1] L. Liu, H. Bai, J. Liu, D.D. Sun, Multifunctional graphene oxide–TiO(2)–Ag nanocomposites for high performance water disinfection and decontamination under solar irradiation, J. Hazard. Mater. 261 (2013) 214–223.
[2] X. Wang, T.T. Lim, Highly efficient and stable Ag-AgBr/TiO_2 composites for destruction of Escherichia coli under visible light irradiation, Water Res. 47 (2013) 4148–4158.
[3] J.S. Lee, K.H. You, C.B. Park, Highly photoactive, low bandgap TiO_2 nanoparticles wrapped by graphene, Adv. Mater. 24 (2012) 1084–1088.
[4] R. Goei, T.T. Lim, Ag-decorated TiO_2 photocatalytic membrane with hierarchical architecture: photocatalytic and anti-bacterial activities, Water Res. 59 (2014) 207–218.
[5] A. Markowska-Szczupak, K. Ulfig, A.W. Morawski, The application of titanium dioxide for deactivation of bioparticulates: an overview, Catal. Today 169 (2011) 249–257.
[6] L. Liu, Z. Liu, H. Bai, D.D. Sun, Concurrent filtration and solar photocatalytic disinfection/degradation using high-performance Ag/TiO_2 nanofiber membrane, Water Res. 46 (2012) 1101–1112.
[7] S. Gurunathan, J.W. Han, A.A. Dayem, V. Eppakayala, J.H. Kim, Oxidative stress-mediated antibacterial activity of graphene oxide and reduced graphene oxide in *Pseudomonas aeruginosa*, Int. J. Nanomed. 7 (2012) 5901–5914.
[8] Z. Chen, Y. Wang, T. Ba, Y. Li, J. Pu, T. Chen, Y. Song, Y. Gu, Q. Qian, J. Yang, G. Jia, Genotoxic evaluation of titanium dioxide nanoparticles in vivo and in vitro, Toxicol. Lett. 226 (2014) 314–319.
[9] S.C. Tang, I.M. Lo, Magnetic nanoparticles: essential factors for sustainable environmental applications, Water Res. 47 (2013) 2613–2632.
[10] M. Auffan, W. Achouak, J. Rose, M.-A. Roncato, C. Chaneac, D.T. Waite, A. Masion, J.C. Woicik, M.R. Wiesner, J.-Y. Bottero, Relation between the redox state of iron-based nanoparticles and their cytotoxicity toward *Escherichia coli*, Environ. Sci. Technol. 42 (2008) 6730–6735.
[11] C.H. Deng, J.L. Gong, G.M. Zeng, C.G. Niu, Q.Y. Niu, W. Zhang, H.Y. Liu, Inactivation performance and mechanism of *Escherichia coli* in aqueous system exposed to iron oxide loaded graphene nanocomposites, J. Hazard. Mater. 276 (2014) 66–76.
[12] Y.P. Huang, B. Chen, F.J. Yao, S.F. Chen, B. Ouyang, C.H. Deng, Y.R. Huang, Weaker masturbatory erection may be a sign of early cardiovascular risk associated with erectile dysfunction in young men without sexual intercourse, J. Sex. Med. 11 (2014) 1519–1526.
[13] S. Pavagadhi, A.L. Tang, M. Sathishkumar, K.P. Loh, R. Balasubramanian, Removal of microcystin-LR and microcystin-RR by graphene oxide: adsorption and kinetic experiments, Water Res. 47 (2013) 4621–4629.
[14] L. Chen, C.H. Deng, F. Guo, Y.J. Tang, J. Shi, L. Ren, Reducing the Fault Current and Overvoltage in a Distribution System With Distributed Generation Units Through an Active Type SFCL, IEEE Trans. Appl. Supercond. 24 (2014).
[15] B.M. Almeida, M.A. Melo Jr., J. Bettini, J.E. Benedetti, A.F. Nogueira, A novel nanocomposite based on TiO_2/Cu_2O/reduced graphene oxide with enhanced solar-light-driven photocatalytic activity, Appl. Surf. Sci. 324 (2015) 419–431.
[16] S. Das, G.C. Nayak, S.K. Sahu, P.C. Routray, A.K. Roy, H. Baskey, Microwave absorption properties of double-layer composites using CoZn/NiZn/MnZn-ferrite and titanium dioxide, J. Magn. Magn. Mater. 377 (2015) 111–116.
[17] J.-H. Deng, X.-R. Zhang, G.-M. Zeng, J.-L. Gong, Q.-Y. Niu, J. Liang, Simultaneous removal of Cd(II) and ionic dyes from aqueous solution using magnetic graphene oxide nanocomposite as an adsorbent, Chem. Eng. J. 226 (2013) 189–200.
[18] Y. Cong, M. Long, Z. Cui, X. Li, Z. Dong, G. Yuan, J. Zhang, Anchoring a uniform TiO_2 layer on graphene oxide sheets as an efficient visible light photocatalyst, Appl. Surf. Sci. 282 (2013) 400–407.
[19] J.-L. Gong, X.-Y. Wang, G.-M. Zeng, L. Chen, J.-H. Deng, X.-R. Zhang, Q.-Y. Niu, Copper (II) removal by pectin–iron oxide magnetic nanocomposite adsorbent, Chem. Eng. J. 185–186 (2012) 100–107.
[20] S.B. Liu, T.H. Zeng, M. Hofmann, E. Burcombe, J. Wei, R.R. Jiang, J. Kong, Y. Chen, Antibacterial activity of graphite, graphite oxide, graphene oxide, and reduced graphene oxide: membrane and oxidative stress, ACS Nano 5 (2011) 6971–6980.
[21] P. Gao, K. Ng, D.D. Sun, Sulfonated graphene oxide–ZnO–Ag photocatalyst for fast photodegradation and disinfection under visible light, J. Hazard. Mater. 262 (2013) 826–835.
[22] B. Cao, S. Cao, P. Dong, J. Gao, J. Wang, High antibacterial activity of ultrafine TiO_2/graphene sheets nanocomposites under visible light irradiation, Mater. Lett. 93 (2013) 349–352.
[23] M.V. Liga, E.L. Bryant, V.L. Colvin, Q. Li, Virus inactivation by silver doped titanium dioxide nanoparticles for drinking water treatment, Water Res. 45 (2011) 535–544.
[24] M. Cho, H.M. Chung, W.Y. Choi, J.Y. Yoon, Different inactivation behaviors of MS-2 phage and *Escherichia coli* in TiO_2 photocatalytic disinfection, Appl. Environ. Microbiol. 71 (2005) 270–275.
[25] R.V. Kumar, G. Raza, Photocatalytic disinfection of water with Ag–TiO_2 nanocrystalline composite, Ionics 15 (2008) 579–587.
[26] C. Jayaseelan, A.A. Rahuman, S.M. Roopan, A.V. Kirthi, J. Venkatesan, S.K. Kim, M. Iyappan, C. Siva, Biological approach to synthesize TiO_2 nanoparticles using *Aeromonas hydrophila* and its antibacterial activity, Spectrochim. Acta A, Mol. Biomol. Spectrosc. 107 (2013) 82–89.
[27] A. Rincon, Effect of pH, inorganic ions, organic matter and H_2O_2 on *E. coli* K12 photocatalytic inactivation by TiO_2 – implications in solar water disinfection, Appl. Catal. B: Environ. 51 (2004) 283–302.

[28] M.G. Kang, H.S. Jung, K.J. Kim, Effect of chloride ions on 4-chlorophenol photodegradation in the absence and presence of titanium silicalite-2, J. Photochem. Photobiol. A-Chem. 136 (2000) 117–123.
[29] S. Sontakke, C. Mohan, J. Modak, G. Madras, Visible light photocatalytic inactivation of *Escherichia coli* with combustion synthesized TiO_2, Chem. Eng. J. 189–190 (2012) 101–107.
[30] D.M. Alrousan, P.S. Dunlop, T.A. McMurray, J.A. Byrne, Photocatalytic inactivation of *E. coli* in surface water using immobilised nanoparticle TiO_2 films, Water Res. 43 (2009) 47–54.
[31] H. Sakai, E. Ito, R.X. Cai, T. Yoshioka, Y. Kubota, K. Hashimoto, A. Fujishima, Intracellular Ca2+ concentration change of T24 cell under irradiation in the presence of TiO_2 ultrafine particles, Biochim. Biophys. Acta 1201 (1994) 259–265.
[32] H. Zheng, P.C. Maness, D.M. Blake, E.J. Wolfrum, S.L. Smolinski, W.A. Jacoby, Bactericidal mode of titanium dioxide photocatalysis, J. Photochem. Photobiol. A-Chem. 130 (2000) 163–170.
[33] T. Saito, T. Iwase, J. Horie, T. Morioka, Mode of photocatalytic bactericidal action of powdered semiconductor TiO_2 on mutans streptococci, J. Photochem. Photobiol. B-Biol. 14 (1992) 369–379.